

Microscopic theories of neutrino- ^{12}C reactions

C. Volpe^a, N.Auerbach^b, G.Colò^c, T.Suzuki^d, N. Van Giai^a

^{a)} *Groupe de Physique Théorique, Institut de Physique Nucléaire, F-91406 Orsay Cedex, France*

^{b)} *School of Physics and Astronomy, Tel Aviv University, Tel Aviv 69978, Israel*

^{c)} *Dipartimento di Fisica, Università degli Studi, via Celoria 16, 20133 Milano, Italia*

^{d)} *Department of Physics, College of Humanities and Science, Nihon University, Sakurajosui 3-25-40, Setagaya-ku, Tokyo 156, Japan*

In view of the recent experiments on neutrino oscillations performed by the LSND and KARMEN collaborations as well as of future experiments, we present new theoretical results of the flux averaged $^{12}\text{C}(\nu_e, e^-)^{12}\text{N}$ and $^{12}\text{C}(\nu_\mu, \mu^-)^{12}\text{N}$ cross sections. The approaches used are charge-exchange RPA, charge-exchange RPA among quasi-particles (QRPA) and the Shell Model. With a large-scale shell model calculation the exclusive cross sections are in nice agreement with the experimental values for both reactions. The inclusive cross section for ν_μ coming from the decay-in-flight of π^+ is $15.2 \times 10^{-40} \text{ cm}^2$ (when Hartree-Fock wavefunctions are used), to be compared to the experimental value of $12.4 \pm 0.3 \pm 1.8 \times 10^{-40} \text{ cm}^2$, while the one due to ν_e coming from the decay-at-rest of μ^+ is $16.4 \times 10^{-42} \text{ cm}^2$ which agrees within experimental error bars with the measured values. The shell model prediction for the decay-in-flight neutrino cross section is reduced compared to the RPA one, namely $19.2 \times 10^{-40} \text{ cm}^2$. This is mainly due to the different kind of correlations taken into account in the calculation of the spin modes (in particular, because of the quenching in the 1^+ channel) and partially due to the shell-model configuration basis which is not large enough, as we show using arguments based on sum-rules. Results for exclusive and inclusive muon capture rates and beta decay are given and are close to the experimental findings.

I. INTRODUCTION

For many years, weak processes in nuclei such as beta decay and muon capture have been studied on the one hand to deepen our knowledge of the weak interaction in nuclei and on the other hand to yield information on nuclear structure. Both aspects are important when one considers other weak processes in nuclei, namely reactions induced by scattered neutrinos. A description of the latter processes is not only important in our attempts to better understand the nature of such reactions but also it has significant practical importance in current experimental studies of neutrinos. In fact, nuclei are often used as neutrino detectors so that the knowledge of reactions induced by neutrinos on nuclei becomes a crucial step for the interpretation of experiments on neutrinos, such as the ones aiming to go beyond the Standard Model looking for neutrino oscillations and masses or those measuring solar neutrinos to test the Standard Solar Model.

A clear example is given by the recent experiments performed both by the LSND and the KARMEN collaborations, looking for $\nu_\mu \rightarrow \nu_e$ [1,2], $\bar{\nu}_\mu \rightarrow \bar{\nu}_e$ [3,4] or $\nu_\mu \rightarrow \nu_x$ [5] oscillations with neutrinos produced by accelerators. The detectors used in these measurements are mainly composed of protons and ^{12}C . Reactions of neutrinos on this nucleus are used to check neutrino fluxes and efficiencies [6]. In the $\nu_e \rightarrow \nu_x$ disappearance experiment of Ref. [5] with ν_e coming from the Decay-At-Rest (DAR) of μ^+ , the charged-current (CC) reaction $\nu_e + ^{12}\text{C} \rightarrow e^- + ^{12}\text{N}_{g.s.}$ is used to detect neutrinos. In Ref. [1] the $\nu_\mu \rightarrow \nu_e$ appearance experiment with ν_μ coming from the Decay-In-Flight (DIF) of π^+ , ^{12}C is used to detect neutrinos via the CC reaction $\nu_e + ^{12}\text{C} \rightarrow e^- + ^{12}\text{N}$. In both cases, the extracted oscillation probabilities rely directly on the knowledge of the cross section for these reactions. The exclusive cross section for $\nu_e + ^{12}\text{C} \rightarrow e^- + ^{12}\text{N}_{g.s.}$ (where ^{12}N is left in the ground state) has been measured by different collaborations [7–9] and its value can be obtained in a model independent way by using form factors deduced from the measurements of related weak processes such as beta decay and muon capture as it is done in the Elementary Particle Theory (EPT) [10]. Concerning the inclusive cross section for $\nu_e + ^{12}\text{C} \rightarrow e^- + ^{12}\text{N}$ (where ^{12}N is left either in the ground state or in an excited state), because of the universality of the weak interaction we expect this reaction to be described by the same effective hamiltonian as the reaction $\nu_\mu + ^{12}\text{C} \rightarrow \mu^- + ^{12}\text{N}$ with ν_μ coming from the DIF of π^+ . A problem concerning this reaction has emerged which has been extensively investigated recently, namely the theoretical cross section overestimates the experimental value [6] by about 50% within charge-exchange RPA [11,12] or by about 30 – 40% in [13]. An attempt has also been made within an extension of the EPT [14], but it is based on several assumptions which have not been tested yet [15]. In a recent shell model calculation [16] the value of the cross section is reduced in apparent agreement with the experimental value. The reaction cross section with neutrinos coming from the DIF of π^+ has been measured only by the LSND collaboration up to now [6,17]. Because the same detector used for these measurements has been used to measure the neutrino oscillations, it is important to know what we can say

about these reaction cross section from the theoretical point of view, keeping in mind that every nuclear structure model necessarily contains approximations.

The weak interaction in nuclei being well known, an accurate prediction of these cross sections is a challenging problem from the nuclear structure point of view. In fact, these observables rely on transition densities which can be obtained only in calculations which take into account the different aspects of the structure of the nuclei involved in these reactions. First, it is known for a very long time [18] that ^{12}C is not a true closed sub-shell nucleus or, in other words, that the ground state wave function can be only described by an intermediate coupling scheme and contains configuration mixing, including deformed components. Second, if on one hand in the DAR experiments the neutrinos have impinging energies of the order of several tens of MeV , in the DIF experiment the energy goes up to around 300 MeV . As a consequence, the DAR reaction cross section is dominated by the Gamow-Teller (GT) transition to the ground state of ^{12}N for which information on the transition probabilities can be obtained from other related weak processes like $^{12}\text{N}(\beta^+)^{12}\text{C}$, $^{12}\text{B}(\beta^-)^{12}\text{C}$ and $^{12}\text{C}(\mu^-)^{12}\text{B}$. On the contrary, in the DIF reaction the energy and momentum transferred to the nucleus is quite large so that ^{12}N can be left in an excited state of several tens of MeV , that is, in and above the giant resonance region. If the transition to $^{12}\text{N}_{gs}$ represents 2/3 of the total reaction cross section in the DAR case, the cross section given by transitions to the excited states is 200 times larger than the transition to the $^{12}\text{N}_{gs}$, if the neutrinos come from the DIF of pions. This means that to have an accurate prediction for these cross sections we need nuclear structure models which are not only capable of taking into account configuration mixing in the ground state wave function of ^{12}C but also of describing high-lying states in ^{12}N . This is a quite difficult task within the present nuclear structure models.

The microscopic theoretical approaches used so far are either the charge-exchange Random-Phase-Approximation (we will call it from now on simply RPA) [19] or the shell model [20]. The former includes only partially configuration mixing in the ground state while it can easily include high-lying one particle-one hole (1p-1h) configurations. On the other hand the shell model can give a good description of the ground state wave function whereas the prediction of other-lying states requires a large model-space which may be very difficult to treat numerically.

In this paper we try to improve the existing calculations within the two microscopic approaches just mentioned. First, we use a charge-exchange RPA approach applied to quasi-particles (we will call it from now on simply QRPA), in order to improve the poor description of the ground state of ^{12}C within RPA. The configuration mixing is introduced by including “*ad hoc*” pairing correlations in this nucleus. This is done to see if the configuration mixing that is missing in the RPA ground state wave function can be at the origin of the discrepancy between the measured reaction cross section and the theoretical predictions as it was first suggested in [12]. It was shown in [12] that the inclusion of fractional occupancies within the RPA approach reduces the exclusive cross section from a factor 3-4 to 50% discrepancy. In Ref. [21] an RPA calculation with partial occupancies was performed and it led to similar results for the exclusive cross section while the inclusive cross section was shown to decrease by a few percent. However, the authors of [12,21] did not show the results of a full QRPA calculation as we do here.

Next, we perform shell model calculations within a large model space. Our space is larger than that actually used in [16] where the results in the same space we use are obtained by extrapolation only. We will compare our results to the experimental findings [6-9,17] and to the other microscopic theoretical predictions [12,16,21]. We will conclude by summarizing the present status of the problem.

In section II we briefly review the general theory describing neutrino scattering on nuclei, muon capture and beta decay. In section III we present the essential features of the microscopic models used in our calculations, i.e. the QRPA and the shell model. In section IV results from the above mentioned weak processes are presented focusing in particular on the cross sections for the reactions $\nu_l + ^{12}\text{C} \rightarrow l + ^{12}\text{N}$ ($l = e, \mu$), both inclusive and exclusive, with ν_e coming from DAR of μ^+ and with ν_μ coming from the DIF of π^+ . Conclusions are drawn in section V.

II. GENERAL THEORY

The theoretical framework to study nuclear responses to weak probes is discussed extensively in the literature. A detailed description can be found in [22]. Here we will just present the main ingredients of the calculation necessary for the discussion.

The general expression for the cross section of the reaction $\nu_l + ^{12}\text{C} \rightarrow l + ^{12}\text{N}$ ($l = e, \mu$) is [23]

$$\sigma = (2\pi)^4 \sum_f \int d^3 p_l \delta(E_l + E_f - E_\nu - E_i) |\langle l(p_l); f | H_{eff} | \nu_l(p_\nu); i \rangle|^2, \quad (1)$$

where E_f (E_i) is the energy of the final (initial) nuclear state, E_ν (p_ν) is the incident neutrino energy (momentum) and E_l (p_l) is the outgoing lepton energy (momentum). The effective single-particle hamiltonian H_{eff} is derived by

carrying out the Foldy-Wouthuysen (FW) transformation and retaining terms up to $O((|\mathbf{q}|/M)^3)$ (M is the nucleon mass and \mathbf{q} is the momentum transfer), since the momentum transfer involved in nuclear scattering of neutrinos produced by accelerators can be large. The expression for H_{eff} can be found in [23]. If the nuclear recoil effects are ignored, we have

$$\sigma = \frac{G^2}{2\pi} \cos^2 \theta_C \sum_f p_l E_l \int_{-1}^1 d(\cos \theta) M_\beta, \quad (2)$$

where $G \cos \theta_C$ is the weak coupling constant, θ is the angle between the directions of the incident neutrino and the outgoing lepton and M_β is given by

$$M_\beta \equiv M_F |\langle f | \tilde{1} | i \rangle|^2 + M_{G0} \frac{1}{3} |\langle f | \tilde{\sigma} | i \rangle|^2 + M_{G2} \Lambda \quad (3)$$

where the squared nuclear matrix elements are

$$|\langle f | \tilde{1} | i \rangle|^2 = \frac{4\pi}{(2J_i + 1)} \sum_l |\langle J_f || \sum_k t_+(k) j_l(qr_k) Y_l(\hat{\mathbf{r}}_k) || J_i \rangle|^2, \quad (4)$$

$$|\langle f | \tilde{\sigma} | i \rangle|^2 = \frac{4\pi}{(2J_i + 1)} \sum_{l,K} |\langle J_f || \sum_k t_+(k) j_l(qr_k) [Y_l(\hat{\mathbf{r}}_k) \times \sigma]^{(K)} || J_i \rangle|^2, \quad (5)$$

$$\begin{aligned} \Lambda &\equiv \left(\frac{5}{6}\right)^{\frac{1}{2}} \sum_{l,l',K} (-1)^{l/2-l'+2+K} \sqrt{2l+1} \sqrt{2l'+1} \begin{pmatrix} l' & 2 \\ 0 & 0 \end{pmatrix} \left\{ \begin{matrix} 1 & 1 & 2 \\ l' & l & K \end{matrix} \right\} \frac{4\pi}{(2J_i + 1)} \\ &\times \langle J_f || \sum_k t_+(k) j_l(qr_k) [Y_l(\hat{\mathbf{r}}_k) \times \sigma]^{(K)} || J_i \rangle \\ &\times \langle J_f || \sum_{k'} t_+(k') j_{l'}(qr_{k'}) [Y_{l'}(\hat{\mathbf{r}}_{k'}) \times \sigma]^{(K)} || J_i \rangle^\dagger. \end{aligned} \quad (6)$$

where k labels the space and spin-isospin coordinates of the k -th nucleon, l, l' are the orbital angular momenta and K is the total angular momentum of the transition operators. The coefficients M_F, M_{G0} and M_{G2} [23] appearing in (3) depend on the momentum transferred to the nucleus ($q = (\mathbf{q}, iq_0) = p_l - p_\nu$) and the standard nucleon form factors $f_V(q^2), f_A(q^2), f_W(q^2), f_P(q^2)$. Second-class current form factors are ignored.

A correction to (2) must be introduced to account for the distortion of the outgoing lepton wave function due to the Coulomb field of the daughter nucleus. For reactions on ^{12}C with neutrinos from the DAR of μ^+ , the quantity $p_l R_A$ (R_A is the radius of the nucleus) is of the order of 0.5. In this case, the cross section (2) may be multiplied by the Fermi function $F(Z_f, E_l)$ [24], where Z_f is the charge of the daughter nucleus and E_l the energy of the charged lepton. When the neutrinos come from the DIF of π^+ , the outgoing muons have $p_l R_A > 0.5$. With relativistic leptons, the effect due to the Coulomb field may be included by using the ‘‘Effective Momentum Approximation’’ (EMA) [25]. In this approximation the lepton energy and momentum are modified by a constant electrostatic potential within the nucleus, i.e. $E_{l,eff} = E_l - V(0)$ and $p_{l,eff} = (E_{l,eff}^2 - m^2)^{1/2}$ with $V(0) = -3Z_f \alpha / 2R$. The cross section (2) has then to be multiplied by a factor $p_{l,eff} E_{l,eff} / (p_l E_l)$.

To obtain the flux-averaged cross sections $\langle \sigma \rangle_f$ that can be compared with the experimental data, the energy dependent cross section (2) has to be folded with the normalized neutrino flux $\tilde{f}(E_\nu)$ (depending on the neutrino source used)

$$\langle \sigma \rangle_f = \int dE_\nu \sigma(E_\nu) \tilde{f}(E_\nu), \quad (7)$$

where

$$\tilde{f}(E_\nu) = \frac{f(E_\nu)}{\int_{E_0}^\infty dE'_\nu f(E'_\nu)}, \quad (8)$$

$f(E_\nu)$ being the initial flux and E_0 the threshold energy.

Closely related to this neutrino capture reaction is the capture of a negative muon bound in an atomic orbit, $\mu^- + (A, Z) \rightarrow (A, Z - 1)^* + \nu_\mu$. In the 1S-capture the inclusive rate Λ_c is given by

$$\Lambda_c = \frac{m_\mu^2}{2\pi} |\phi_{1S}|^2 [G_V^2 M_V^2 + G_A^2 M_A^2 + (G_P^2 - 2G_P G_A) M_P^2]. \quad (9)$$

if we neglect the recoil term which represents a correction of a few percent [26]. The function ϕ_{1S} is the muon 1S-bound state wave function evaluated at the origin, i.e., $|\phi_{1S}|^2 = R(Z\alpha m')^3/\pi$, R being a reduction factor accounting for the finite size of the nuclear charge distribution ($R = 0.86$ for ^{12}C) [22] and m' the muon reduced mass. The constants G_V, G_A, G_P [27] are the ‘‘effective coupling constants’’ which depend only slightly on the neutrino momentum p_ν . This can be simply obtained from the energy and momentum conservation, $p_\nu = m' - (m_n - m_p) - |E_\mu^B| - E_{fi}$, where m_n, m_p are the neutron and proton masses, $|E_\mu^B|$ is the binding energy of the muon in the 1S orbit and E_{fi} is the nuclear excitation energy measured with respect to the parent nucleus ground state. The capture rate can be factorized as in (9) if we neglect the dependence of the coupling constants on p_ν . The square of the vector, axial-vector and pseudoscalar matrix elements are

$$M_V^2 = 4\pi \sum_l (2l+1) \sum_f \left(\frac{p_\nu}{m_\mu}\right)^2 |\langle J_f | \sum_k t_+(k) j_l(p_\nu r_k) Y_{l0}(\hat{\mathbf{r}}_k) | J_i \rangle|^2, \quad (10)$$

$$M_A^2 = 4\pi \sum_{l,K} (2K+1) \sum_f \left(\frac{p_\nu}{m_\mu}\right)^2 |\langle J_f | \sum_k t_+(k) j_l(p_\nu r_k) [Y_l(\hat{\mathbf{r}}_k) \times \sigma]^{K0} | J_i \rangle|^2, \quad (11)$$

$$M_P^2 = 4\pi \sum_{l,l',K} (2K+1) \sum_f \left(\frac{p_\nu}{m_\mu}\right)^2 |\langle J_f | \sum_k t_+(k) \theta_P(K) | J_i \rangle|^2, \quad (12)$$

where

$$\theta_P(K) = \left\{ \sqrt{\frac{K}{(2K+1)}} j_l(p_\nu r_k) [Y_l(\hat{\mathbf{r}}_k) \times \sigma]^{K0} + \sqrt{\frac{(K+1)}{(2K+1)}} 2j'_l(p_\nu r_k) [Y_{l'}(\hat{\mathbf{r}}_k) \times \sigma]^{K0} \right\}. \quad (13)$$

with $l = K - 1$ and $l' = K + 1$. The β -decay corresponds to the limit of zero momentum transfer of the transition probabilities in (3), that is

$$M_\beta^0 \equiv f_V^2(0) |\langle f | 1 | i \rangle|^2 + f_A^2(0) \frac{1}{3} |\langle f | \sigma | i \rangle|^2 \quad (14)$$

where

$$|\langle f | 1 | i \rangle|^2 = \frac{1}{2J_i + 1} |\langle J_f | \sum_k t_+(k) | J_i \rangle|^2 \quad (15)$$

$$|\langle f | \sigma | i \rangle|^2 = \frac{1}{2J_i + 1} |\langle J_f | \sum_k t_+(k) \sigma(k) | J_i \rangle|^2 \quad (16)$$

and the transition operators are of the usual Fermi or Gamow-Teller type. The ft value is given by

$$ft = \frac{2\pi^3 \ln 2}{(G^2 \cos^2 \theta_C m_e^5)} \frac{1}{M_\beta^0}. \quad (17)$$

The neutrino reaction cross section (2), the muon capture rate (9) and the ft value for the beta decay (14) depend on the wavefunctions of the initial and final nuclear states involved in these processes. The microscopic models used in this work to evaluate these wavefunctions and the corresponding transition probabilities are described in the next section.

III. MICROSCOPIC MODELS

A. RPA and QRPA

Transition matrix elements of the type entering in eqs. (3,9,14) can be calculated within the framework of RPA or QRPA. In the present work, the starting point is a Hartree-Fock (HF) calculation of the ground-state of ^{12}C , performed in coordinate space by using the Skyrme-type effective interactions SIII [28] and SGII [29]. The SGII force was built with the purpose of obtaining a proper description of spin-isospin nuclear properties. The HF solution determines the mean-field and single-particle (s.p.) occupied levels of ^{12}C which has a closed-subshell structure in this description. The unoccupied levels of ^{12}C are obtained by diagonalizing the HF mean-field using a harmonic oscillator basis. Therefore, the continuum part of the s.p. spectrum is discretized and discrete particle-hole (ph) configurations coupled to J^π are used as a basis in order to cast the RPA equations in the matrix form. The details of this procedure can be found in [30]. This RPA calculation is self-consistent since the residual interaction among ph states is derived from the same Skyrme force used to produce the mean field.

To go beyond the closed-subshell approximation for the ^{12}C ground state, pairing correlations are taken into account in the HF+BCS approximation. Constant pairing gaps Δ_p and Δ_n for protons and neutrons are introduced and are set at 4.5 MeV. A large pairing gap is unrealistic for states far from the Fermi surface, and an energy cut-off is required, such that the states above this cut-off have $\Delta = 0$. The cut-off is set at the $2s_{1/2}$ state. On top of the HF+BCS calculation, the QRPA matrix equations can be written with a procedure which parallels what was described above, with the two-quasiparticle (2qp) configurations replacing the ph ones. We do not present here the details of the QRPA formalism, which is found in the literature (see, e.g., Ref. [31]). We simply note that the particle-particle matrix elements are here renormalized by means of a parameter g_{pp} that has been chosen to be smaller than 1 (typically 0.7) to avoid the well-known ground-state instabilities.

For the multipolarities studied, it is found that the space used for the RPA (QRPA) calculations satisfies well (up to a few percent) the energy-weighted sum rule (EWSR) associated with the operators of the type

$$\sum_k t_+(k) r_k^l Y_l(\hat{\mathbf{r}}_k), \quad \sum_k t_+(k) r_k^l [Y_l(\hat{\mathbf{r}}_k) \times \sigma]^{(J)} \quad (18)$$

which are the small- q limit of those defined in the preceding section.

For each multipolarity, every eigenstate of the RPA or QRPA equations is characterized by its X^f and Y^f amplitudes and the transition matrix element for a generic operator $\hat{O}(k)$ is written as

$$\langle J_f | \sum_k \hat{O}(k) | J_i \rangle = \sum_{\alpha, \beta} \langle \alpha | \sum_k \hat{O}(k) | \beta \rangle (X_{\alpha\beta}^f u_\alpha v_\beta + Y_{\alpha\beta}^f v_\alpha u_\beta), \quad (19)$$

where α and β label a given ph or 2qp states, u and v are the BCS occupation amplitudes (which reduce to 1 and 0 in the HF-RPA case) and $\langle \alpha | \sum_k \hat{O}(k) | \beta \rangle$ are single-particle matrix elements. With $\Delta = 4.5 \text{ MeV}$, the occupation probabilities for the $1p_{3/2}$ and $1p_{1/2}$ states are $v_{p_{3/2}}^2 = 0.84$ and $v_{p_{1/2}}^2 = 0.19$ respectively. The latter one is smaller than the one used in [12,21].

B. Shell Model

We also evaluate transition matrix elements for neutrino and muon capture reactions using a large shell model space. It is desirable to use extended spaces as much as possible in order to treat both inclusive and exclusive reactions. Here, we take the $0s-0p-1s0d-1p0f$ shell model space and include configurations up to $3\hbar\omega$ excitations for negative parity states and up to $2\hbar\omega$ excitations for positive parity states. No ^4He core is assumed in the present calculations. The configurations taken for positive parity states in $A=12$ nuclei are

$$(0s)^4(0p)^8 + (0s)^4(0p)^6(1s0d)^2 + (0s)^4(0p)^7(1p0f)^1 \\ + (0s)^3(0p)^8(1s0d)^1 + (0s)^2(0p)^{10} \quad (20)$$

and those for negative parity states are

$$(0s)^4(0p)^7(1s0d)^1 + (0s)^3(0p)^9 + (0s)^4(0p)^6(1s0d)^1(1p0f)^1 \\ + (0s)^4(0p)^5(1s0d)^3 + (0s)^3(0p)^8(1p0f)^1 \\ + (0s)^3(0p)^7(1s0d)^2 + (0s)^2(0p)^9(1s0d)^1 \quad (21)$$

In the shell model calculations of ref. [16] of the present problem, computations were carried out with configurations up to $1\hbar\omega$ excitation for negative parity states and up to $2\hbar\omega$ excitation for positive parity states.

The spurious center-of-mass states are eliminated here by using the method of Lawson [32]. The spurious states are pushed up to higher energies with the addition of a fictitious term in the hamiltonian which acts only on the center-of-mass excitations. The number of spurious states removed is $\sim 1000 - 4000$ for each negative parity multipole ($0^-, \dots, 4^-$) and $\sim 100 - 400$ for each positive parity multipole ($0^+, \dots, 6^+$). The number of states (without the spurious center-of-mass components) amounts to $\sim 2800 - 10600$ for the negative parity multipoles and $\sim 250 - 1500$ for the positive parity multipoles. The number of states is very large for the negative parity multipoles compared to the work in ref. [16], in which the number was $\sim 50 - 150$ and included up to $1\hbar\omega$ excitation only.

We adopt here the effective interaction of Warburton and Brown [33] for use in the present $0s-0p-1s0d-1p0f$ model space, and we use the set WB10 [34], which is based on the WBT interaction [33]. This interaction was obtained by fitting binding energies and energy levels, including cross-shell data. The interaction describes well the low excitation energy spectra for $A= 10-22$ nuclei. It has also been used to investigate Gamow-Teller β decay rates for $A \leq 18$ nuclei [35].

In the shell model, the reduced matrix elements of transition operators are expressed as linear combinations of the reduced matrix elements of single-particle states with coefficients given by one-body density matrix elements

$$\langle J_f T_f || \hat{O}^{\lambda t} || J_i T_i \rangle = \sum_{j_i j_f} C_{j_i j_f}^{\lambda t} \langle j_f || \hat{O}^{\lambda t} || j_i \rangle. \quad (22)$$

The form factors in (3) have to be corrected for the center-of-mass motion. This is done by multiplying the matrix elements by the Tassie-Barker function, $\exp(b^2 q^2 / 2A)$, with b being the oscillator length parameter [36].

IV. DISCUSSION OF THE RESULTS

A. Theory versus experiment

Using the above formalism we calculate results for the flux-averaged cross sections for neutrinos coming from the DIF of π^+ , $(\nu_\mu, \mu^-)DIF$, and for neutrinos coming from the DAR of μ^+ , $(\nu_e, e^-)DAR$. The flux-averaged cross sections are obtained by taking neutrino fluxes from [37]. As far as RPA and QRPA are concerned, we discuss in the following results obtained by using the force SIII. We have checked that the interaction SGII gives very similar results.

Let us first discuss our results for the inclusive cross sections (table I). In the Shell Model (SM) case, cross sections obtained both in the $0s-0p-1s0d$ ($(0+1+2)\hbar\omega$) model space and in the $0s-0p-1s0d-1p0f$ ($(0+1+2+3)\hbar\omega$) model space are shown. Results in the smaller space are only given for comparison with [16]. Two different types of radial wavefunctions have been used, the Harmonic Oscillator with $b = 1.64 fm$ (HO wf) and Hartree-Fock wavefunctions (HF wf). HO wavefunctions are used even though their radial behaviour is known not to give good results of $^{12}C(p, n)$ reactions cross sections. The reason for using them is twofold : i) the spurious center-of-mass motion is exactly subtracted only in this case; ii) they are employed in order to show the sensitivity of the calculated cross sections to the choice of the radial wavefunctions. Cross sections can be indeed quite sensitive to the radial wavefunctions since going from HO to HF wavefunctions in the $(\nu_\mu, \mu^-)DIF$ case produces changes of about 30%, whereas in the $(\nu_e, e^-)DAR$ case we have variations of a few percent only (see table I). For comparison we also show the results of ref. [16] obtained by extrapolation in the $0s-0p-1s0d-1p0f$ space with Woods-Saxon wave functions. The results obtained within the Skyrme RPA and QRPA are larger than in SM. The QRPA values are slightly larger than the RPA ones for the inclusive cross section. This is due to the fact that in QRPA the particle-particle residual interaction (on the average attractive) competes with the (on the average repulsive) particle-hole residual interaction. As a consequence, the QRPA strength distribution is slightly shifted towards lower energies. This fact produces a few percent increase of the flux-averaged cross sections due to the dependence of the differential cross sections (2) on the energy and momentum of the outgoing lepton and also due to the flux averaging (7,8). In ref. [12,21], on the contrary the introduction of fractional occupancies shifts the strength distribution to higher energies and this gives a few percent decrease of the flux averaged cross section with respect to their RPA results. From table I, we see that the $(\nu_\mu, \mu^-)DIF$ cross sections are compatible with those of ref. [21], but there is a ratio of about a factor 3 for the $(\nu_e, e^-)DAR$ case. Most of the disagreement is due to the bad description of the ground state to ground state transition (its contribution represents 2/3 of the total cross section), some of it arises because of the ground state energy of ^{12}N which is not close to the experimental value. In [21] the single particle energies were fitted to the experimental values whereas our single particle energies are kept as they come out from our Skyrme HF or HF-BCS calculation. The single particle energies are particularly important to get the energy of the ^{12}N ground state with respect to ^{12}C ground state close to its

experimental value of 17.338 MeV . In fact, within RPA this transition corresponds to the $1p_{3/2} \rightarrow 1p_{1/2}$ transition, and with the Skyrme forces employed in this work the energy of this transition is 13.4 MeV .

In table II, we see the importance of including configuration mixing as well as of having the energy of this transition close to its experimental value. This can also be seen from table III, where we give the inclusive $(\nu_e, e^-)DAR$ cross sections calculated without the contribution of the ground state to ground state transition. In this case, our RPA cross section is very close to the experimental value as found in [12,21].

We discuss now the theoretical predictions versus the experimental findings. For the $(\nu_\mu, \mu^-)DIF$ case, we see from table I that our results within SM (with HF wf) are close to the experimental value when the error bars are taken into account, slightly overestimating it. The WS results in [16] agree even better. On the other hand, the RPA, the QRPA and Continuum RPA (CRPA) with fractional occupancies [21] overestimate the experimental value by about 50%. Concerning the $(\nu_e, e^-)DAR$ cross sections, we see that the SM results ($0s-0p-1s0d-1p0f$ with HF wf) are compatible with the experimental values when error bars are taken into account, as those of ref. [16]. Again the CRPA results of ref. [21] overestimate the experimental values by about 30% (while our RPA predictions are far off for the reasons explained above).

Let us discuss the exclusive cross sections together with various related processes like β decay and muon capture. First, we can see from table II that our shell model results nicely agree with the experimental values for both the DIF and the DAR cases. The calculated values are not very sensitive to the choice of the radial wave functions and confirm those calculated in [16]. Our RPA prediction for the $(\nu_\mu, \mu^-)DIF$ is about a factor 3 larger than the experimental value as found also in [11], whereas the introduction of fractional occupancies brings the RPA predictions close to the experimental value [12,21]. As far as the QRPA is concerned, the value obtained is slightly lower than in RPA, but within QRPA there are difficulties in choosing the ground state of ^{12}N because the lowest state is not the most collective one. Therefore all the results concerning the exclusive transition have been obtained by summing the strength of the energy levels within the first 3 MeV above the lowest state and attributing it to a single state at an average energy which is not much different from the RPA one. Our RPA $(\nu_e, e^-)DAR$ exclusive cross section results are a factor 4-5 larger than the experimental values as found in [11]. A related process is the $^{12}N \rightarrow ^{12}C \beta^+$ decay. In this case the transition operator does not have a radial dependence. From table IV, we see that the SM ft value is in reasonable agreement with the experimental one whereas RPA gives values four times smaller as it is well known [11,21]. The ft value for the β^- decay from ^{12}B to ^{12}C is not given, but similar arguments hold since ^{12}B and ^{12}N are mirror nuclei. Finally, let us look at the exclusive muon capture rates (table V). The SM results are very close to the experimental value in agreement with what was found in [16] while as in [21] RPA overestimates it by about a factor 4. The nice agreement between experiment and theory obtained within SM (at variance with standard RPA) shows clearly that the inclusion of configuration mixing is necessary for a good description of the mentioned processes.

We now turn to the discussion of the inclusive $(\nu_e, e^-)DAR$ cross section without the contribution of the ground state to ground state transition (see table III). There are two main differences with the results in [16] : i) our $(\nu_e, e^-)DAR$ cross sections are not very sensitive to the choice of the wavefunctions; ii) the calculated value is twice the one obtained in [16]. In order to understand point i), we show the strength distribution obtained for the multipolarity $J^\pi = 1^+$, calculated either with HO or HF wavefunctions, with $q = 0.2 \text{ fm}^{-1}$ in (5) as a “typical” value of the momentum transferred in the $(\nu_e, e^-)DAR$ reaction (fig.1) and $q = 1.0 \text{ fm}^{-1}$ as a “typical” value for the $(\nu_\mu, \mu^-)DIF$ case (fig.2). We see that the strength distributions obtained for $q = 0.2 \text{ fm}^{-1}$ are the same for the two s.p. wavefunctions, while for $q = 1.0 \text{ fm}^{-1}$ there are significant differences. This explains the sensitivity to the choice of the wavefunctions of the results of table I and III. Concerning point ii), from (2) we see that the differential cross sections scale as the square of the lepton energy in the case of electrons (because of its negligible mass). As a consequence, small shifts in the strength distributions can have large effects on the cross sections as we have already seen in table II. Because neutrino-nucleus reactions with electronic neutrinos are so sensitive to the details of the strength distribution, they could eventually be used as a probe of nuclear structure.

Inclusive muon capture rates, calculated according to (9)-(12) are given in table VI. The SM results in the large space and with HF wavefunctions are about 20% lower than in [16] and 10% lower than the experimental values. Concerning the results obtained within RPA, the disagreement between calculations (present results and ref. [21]) and the experimental value is again due to the bad description of the ground states, as it can be seen from table V.

The contributions of the most important multiplicities with $J \leq 6$ included in the inclusive $(\nu_\mu, \mu^-)DIF$ and $(\nu_e, e^-)DAR$ cross sections are shown in tables VII and VIII respectively. We see that the contributions in RPA and QRPA are essentially the same, showing that the configuration mixing induced by the pairing correlations is not affecting very much the inclusive cross sections. In table VII the results of the SM calculations again depend significantly on the choice of the s.p. wavefunctions. Significant differences are also evident going from RPA to SM (HF wavefunctions), for example for the 1^+ , 1^- , 2^+ and 3^- . On the contrary, the contributions of the different multiplicities to the $(\nu_e, e^-)DAR$ cross sections are almost equal in the three approaches, except for the remarkable difference associated with the 1^+ states (and in particular with the ground state to ground state contribution).

In view of future experiments using ^{12}C as detector for neutrinos, with impinging neutrino fluxes different from the

ones used up to now, in figs.3 and 4 we give the differential cross sections obtained both in RPA and in SM for the reactions $^{12}C(\nu_e, e^-)^{12}N$ and $^{12}C(\nu_\mu, \mu^-)^{12}N$ as a function of neutrino energies up to 300 MeV.

A question arises concerning the reason for the difference between the RPA and SM results for the inclusive cross section in the $(\nu_\mu, \mu^-)DIF$ case (tables I,VII), the value of which has important implications on the recent measurements of neutrino oscillations. The two approaches have two major differences : i) the type of correlations included; ii) the model space used. Concerning point i), we have already seen in the previous section that correlations are actually responsible for the quenching in the 1^+ (ground state to ground state) contribution (table VII) which is taken into account more correctly in the SM. Due to the tensor interaction the effects of quenching and fragmentation of the strength are also important for the spin-dipole mode, especially for the 1^- component (see the discussion in ref. [38]). The difference of cross sections between SM and RPA in the case of the 0^- and 2^- is rather small, while it is about $0.5 \times 10^{-40} \text{ cm}^2$ for the 1^- . The difference in the type of the correlations included explains half of the discrepancy between the SM and RPA results. Concerning ii), one important constraint on nuclear models is due to sum rules [39]. The existence of sum rules imposes constraints on the model spaces to be used in a given approach because one should ensure that the model space used is large enough to satisfy the corresponding sum rule for a given operator. This has not been considered in previous studies [11,16,21] and can explain some of the difference between the RPA and SM cross sections. In the next subsection we discuss the role of sum rules.

B. Sum rules

The processes studied involve operators of two kinds, either of Fermi type (4) or of Gamow-Teller type (5). In the low- q limit these operators become the standard multipole operators (18). As an example we have calculated sum rules for the non spin-flip states $J^\pi = 1^-$ and $J^\pi = 2^+$ both in RPA and in SM. We have found that if for the 1^- states, the corresponding sum rule is satisfied in the two approaches, the sum rule for the 2^+ states is satisfied in the RPA whereas 20% is missing in SM when the largest space ($0s-0p-1s0d-1p0f$) is used. Figure 5 shows a comparison between the RPA and SM strength distributions obtained for the 2^+ states with the Fermi type operator, $\hat{O} = \sum_k r_k^2 Y_2(r_k) t_+(k)$. We can see that in the SM calculation some strength is missing at about 40 – 60 MeV because of the truncation of the space. This missing strength at high energy gives a significant contribution to the flux averaged $(\nu_\mu, \mu^-)DIF$ cross section.

In order to show this we have performed an RPA calculation of this cross section in the same space as used in the SM calculations ($0s-0p-1s0d-1p0f$). The results obtained in RPA, RPA in the restricted ($3\hbar\omega$) model space and SM are shown in table IX. We see that for the 1^- states, for which the basis is large enough for the sum rule to be satisfied, the corresponding cross sections are practically the same in the three cases. On the contrary, the 2^+ contributions to the total cross section look quite different, showing a reduction of about 10% going from RPA to RPA in the restricted space and to almost 30% in the SM. This reduction is due to the missing strength as illustrated in figure 5 and is accompanied by sum rules that are not exhausted.

Finally, from table IX we also see that restricting the RPA space brings the total flux averaged cross section very close to the SM one. This important result seems to indicate strongly that getting theoretical predictions in the shell-model framework which come close to the experimental values in the inclusive $(\nu_\mu, \mu^-)DIF$ can be an artifact because the model spaces used for the calculations are not large enough to satisfy sum rules. When a more extended space is used, it is quite possible that the shell model cross section will increase approaching the RPA value and exceeding the experimental LSND result. However, we should also note that the increase of cross sections with increasing configuration space is not the same for SM and RPA. The rate of increase of cross sections is smaller for the SM case. This can be already seen from the difference of the rate of increase when going from $1\hbar\omega$ to $3\hbar\omega$ spaces when we compare our SM results with ref. [16]. The rate of increase is 14% in our case while it is 19% in ref. [16], where the cross section for $3\hbar\omega$ space was obtained from an extrapolation based on an RPA-like model.

C. The problem of quenching of spin strength

Finally, we would like to discuss more the problem of quenching of spin strength in nuclei. It is known for sometime that there is not enough strength in the main GT peak. Two explanations on the origin of this quenching have been suggested : i) the missing strength is shifted to very high energy due to the coupling of the nucleon internal structure to the Delta resonance; ii) there is a shift of the strength to energies up to about, or more than 50 MeV due to the coupling to multi-particle multi-hole configurations. The quenching and fragmentation of the spin strength due to these effects would lead to quenching of the cross sections of the GT mode and probably for the spin-dipole modes as well. We have made a test calculation in which we have introduced an effective axial vector coupling constant,

g_A^{eff} . Considering high energies of neutrinos in the DIF experiments most of the missing strength due to the above multiparticle effects is picked up and also some portion of the strength due to the coupling to the Delta-Resonance effect is recovered [40,41]. Therefore the g_A^{eff} one should use here should be closer to g_A as compared to the value found for the main GT peak ($g_A^{eff} = 0.8g_A$).

In table X, we show all the results concerning the different processes using a quenching factor. For the sake of demonstration we use $g_A^{eff} = 0.9g_A$. Using this value, the ft value is increased as expected by 20% and the exclusive and inclusive muon capture is reduced by about 15 – 20%. Concerning the exclusive cross sections are reduced by about 15% and become smaller than the observed ones, whereas the inclusive ones are reduced by about 10 – 15% and get closer to the experimental values. The exclusive neutrino cross sections we have seen are very sensitive to the calculated wavefunctions and therefore cannot be a good test of the quenching factor. The inclusive cross sections are less sensitive to nuclear structure and they seem to favor some reduction in g_A . There are many uncertainties in these arguments. We do not yet know for sure what is the mechanism of quenching of g_A (although the experiment in [45] suggests that the main role is played by the coupling with many particle-many hole states) and whether the same quenching factor should be applied to all multiplicities. It is quite conceivable that future studies of the neutrino-nucleus interaction will actually help to clarify this point about quenching.

V. CONCLUSIONS

Microscopic approaches, namely charge-exchange RPA, charge-exchange QRPA and Shell Model, are used to evaluate $^{12}C(\nu_e, e^-)^{12}N$ and $^{12}C(\nu_\mu, \mu^-)^{12}N$ cross sections both for ν_e coming from the decay-at-rest of μ^+ and for ν_μ coming from the decay-in-flight of π^+ . Accurate knowledge of these cross sections is important for the interpretation of recent measurements of neutrino oscillations performed both by LSND and KARMEN collaborations and also for future experiments. The results show that the calculated exclusive cross sections, where ^{12}N is left in the ground state, are in good agreement with the measured values when large-scale shell model calculations are performed. In fact, in this framework it is easy to include properly the configuration mixing present in the ground state of ^{12}C and therefore to have a good description of the ground state wavefunctions. Concerning the inclusive $^{12}C(\nu_\mu, \mu^-)^{12}N$ cross sections with ν_μ from DIF of π^+ , in which ^{12}N is left either in the ground state or in an excited state, we get in the shell model $15.2 \times 10^{-40} \text{ cm}^2$ (when Hartree-Fock wavefunctions are used), about 20% larger than the experimental value, which is $12.4 \pm 0.3 \pm 1.8 \times 10^{-40} \text{ cm}^2$. The calculated cross section in charge-exchange RPA is 50% larger than this value, namely $19.2 \times 10^{-40} \text{ cm}^2$. The most important difference between the SM and RPA is the quenching in the 1^+ due to the different correlations included in the two approaches. This explains half of the difference between the two results. The evaluation of sum rules for natural parity states has also shown that the basis used in the shell model calculations is not large enough to exhaust these sum rules whereas in the case of the RPA the sum rules are satisfied. This fact suggests that the reduced cross section obtained in the shell model framework is partially due to the use of a basis which is not large enough. Enlarging the model space would then add some strength at high energy and therefore increase the inclusive cross sections. From these arguments, we conclude that in both microscopic approaches the theoretical prediction is 20 – 30% larger than the measured value. But even if we could hope to extend further the shell model calculation and increase the basis, the calculated value will keep having 10 – 20% uncertainty due to a certain degree of arbitrariness in the choice of the wavefunctions for the unbound states and also of the interactions. It would be interesting to extend the shell model calculations to larger configuration space in spite of the uncertainties above, to have more information on the correlations in spin-dipole modes and clarify the convergence of the cross sections as the space is extended. Concerning the inclusive $^{12}C(\nu_e, e^-)^{12}N$ cross section we get $16.4 \times 10^{-42} \text{ cm}^2$ which agrees within the experimental error bars with the measured value. The ft value for the beta decay from ^{12}N to ^{12}C , exclusive and inclusive muon capture rates $^{12}B(\mu^-, \nu_\mu)^{12}C$ are also evaluated and are in quite good agreement with the measured values.

This work was supported by the US-Israel Binational Science Foundation. The shell model calculation was done by using the TKYNT at Department of Physics, University of Tokyo.

-
- [1] C.Athanassopoulos and the LSND collaboration, Phys. Rev. Lett. **81**,1774 (1998); C.Athanassopoulos and the LSND collaboration, Phys. Rev. C **58**,2489 (1998).
- [2] K.Eitel, "Proceedings of the 32nd Rencontres de Moriond, Electroweak Interactions and Unified Theories", Les Arcs, 15th-22nd March 1997.
- [3] C.Athanassopoulos and the LSND collaboration, Phys. Rev. Lett. **77**,3082 (1996); C.Athanassopoulos and the LSND collaboration, Phys. Rev. Lett. **75**,2650 (1995).
- [4] K.Eitel and B.Zeitnitz for the KARMEN collaboration, Nucl.Phys.Proc.Suppl. **77**,212 (1999).
- [5] B.Armbruster and al., Phys.Rev.**C57**,3414 (1998).
- [6] C.Athanassopoulos and the LSND collaboration, Phys. Rev. C **56**,2806 (1997); M.Albert and al., Phys. Rev. C **51**,R1065 (1995).
- [7] C.Athanassopoulos and the LSND collaboration, Phys. Rev. C **55**,2078 (1997).
- [8] D.A.Krauker and al., Phys. Rev. C **45**,2450 (1992); R.C.Allen and al., Phys. Rev. Lett. **64**,1871 (1990).
- [9] B.E.Bodmann and the KARMEN collaboration, Phys. Lett. **B332**,251 (1994); J.Kleinfeller and al., in *Neutrino '96*, eds. K.Enquist,H.Huitu and J.Maalampi (World Scientific Singapore, 1997).
- [10] M.Fukugita, Y.Kohyama and K.Kubodera, Phys. Lett. **B212**,139 (1988); Prog. Theor. Phys. **70**,892 (1983).
- [11] E.Kolbe,K.Langanke,F.K.Thielemann and P.Vogel, Phys. Rev. **C52**,3437 (1995); E.Kolbe, K.Langanke and S.Krewald, Phys. Rev. **C49**,1122 (1994).
- [12] N.Auerbach,N.Van Giai and O.K.Vorov, Phys. Rev. **C56**,R2368 (1997).
- [13] S.K.Singh,N.C.Mukhopadyhay and E.Oset, Phys. Rev. C **57**,2687 (1998).
- [14] C.W.Kim and S.L.Mintz, Phys. Rev. C **31**,274 (1985); S.L.Mintz and M.Pourkaviani, Nucl.Phys. **A594**,346 (1995).
- [15] E.Kolbe,K.Langanke and P.Vogel, Nucl. Phys. **A613**,382 (1997).
- [16] A.C.Hayes and I.S.Towner, nucl-th/9907049.
- [17] R.Imlay, Nucl.Phys. **A629**,531c (1998).
- [18] S.Cohen and D.Kurath, Nucl.Phys.**73**,1 (1965).
- [19] N.Auerbach and A.Klein, Nucl.Phys. **A395**,77 (1983).
- [20] Kris L.G. Heyde, " *The nuclear shell model* ", ed. Springer-Verlag (1990).
- [21] E.Kolbe,K.Langanke and P.Vogel, Nucl. Phys. **A652**,91 (1999).
- [22] J.D.Walecka in " *Muon Physics* ", ed. V.M.Hughes and C.S.Wu (Academic, New York, 1975), Vol.II; H.Überhall, B.A.Lamers, J.B.Langworthy and F.J.Kelly, Phys. Rev. C **6**,1911 (1972); J.S.O'Connell, T.W.Donnely and J.D.Walecka, *ibid* **6**,719 (1972).
- [23] T.Kuramoto,M.Fukugita,Y.Kohyama and K.Kubodera, Nucl. Phys. **A512**,711 (1990).
- [24] D.H.Wilkinson and B.E.F.Macefield, Nucl. Phys.A232,58 (1974).
- [25] J.Engel, Phys. Rev. C **57**,2004 (1998).
- [26] N.Auerbach and A.Klein,Nucl. Phys. **A422**,480 (1984).
- [27] J.R.Luyten, H.P.C. Rood and H.A. Tolhoek, Nucl.Phys. **41**,236 (1963).
- [28] M. Beiner, H. Flocard, N. van Giai and Ph. Quentin, Nucl. Phys. **A238**,29 (1975).
- [29] N. Van Giai and H. Sagawa, Phys. Lett. **106**,379 (1981).
- [30] G. Colò, N. Van Giai, P.F. Bortignon and R.A. Broglia, Phys. Rev. **C50**,1496 (1994).
- [31] K. Grotz and H.V. Klapdor, "The weak interaction in nuclear, particle and astrophysics", Adam Hilger, Bristol (1990).
- [32] D.H.Gloeckner and R.D.Lawson, Phys. Lett. **53B**,313 (1974).
- [33] E.K.Warburton and B.A.Brown, Phys.Rev.**C46**,923 (1992).
- [34] OXBASH, The Oxford, Buenos-Aires, Michigan State, Shell Model Program, B. A. Brown, A. Etchegoyen and W. D. M. Rae, MSU Cyclotron Laboratory Report No. 524, 1986.
- [35] W.-T. Chou, E. K. Warburton and B. A. Brown, Phys. Rev. **C47**,163 (1993).
- [36] L.J.Tassie and F.C.Barker, Phys. Rev. **111**,940 (1958).
- [37] R.Imlay, private communication.
- [38] T. Suzuki and H. Sagawa, Nucl. Phys. **A637**,547 (1998).
- [39] E.Lipparini and S.Stringari, Phys.Rep.**175**,103 (1989).
- [40] A. Arima, K. Shimizu, W. Bentz and H. Hyuga, Advances in Nuclear Physics, Vol. 18, Edited by J. W. Negele and E. Vogt, (Plenum, 1987) 1.
- [41] I. S. Towner, Phys. Reports **C155**,263 (1987).
- [42] F.Ajzenberg-Selove, Nucl. Phys. **A433**,1 (1985).
- [43] G.H.Miller and al., Phys. Lett. **B41**,50 (1972).
- [44] T.Suzuki and al., Phys. Rev. **C35**,2212 (1987) and refs. therein.
- [45] T.Wakasa and al., Phys. Rev. **C55**(1997)2909.

TABLE I. Flux averaged inclusive cross sections $\langle \sigma \rangle_f$ within the different approaches used, namely the Shell Model (SM), the Random Phase Approximation (RPA) and the Quasi-particle RPA (QRPA). Different SM results are given according to various choices of radial wavefunctions, i.e., oscillator functions with length parameter $b = 1.64 \text{ fm}$ (HO wf) and Hartree-Fock wave functions (HF wf) and for either $(0 + 1 + 2)\hbar\omega$ or $(0 + 1 + 2 + 3)\hbar\omega$ model space. Comparison with CRPA with fractional occupancies [21] and a recent shell model calculation [16] is made. In the former case the results are obtained with the finite-range G-matrix derived from the Bonn NN potential (BP) and with the Landau-Migdal (LM) force (in brackets). In the latter case, Woods-Saxon wavefunctions (WS wf) have been used and the results within the $(0 + 1 + 2 + 3)\hbar\omega$ model space (in brackets) are obtained by extrapolation.

	$(\nu_\mu, \mu^-)DIF$ $\langle \sigma \rangle_f (10^{-40} \text{ cm}^2)$	$(\nu_e, e^-)DAR$ $\langle \sigma \rangle_f (10^{-42} \text{ cm}^2)$
SM(HO wf) $(0 + 1 + 2)\hbar\omega$	18.71	14.21
SM(HF wf) $(0 + 1 + 2)\hbar\omega$	13.33	13.94
SM(WS wf) $(0 + 1 + 2)\hbar\omega$ [16]	11.1	12.1
SM(HO wf) $(0 + 1 + 2 + 3)\hbar\omega$	21.08	16.70
SM(HF wf) $(0 + 1 + 2 + 3)\hbar\omega$	15.18	16.42
SM(WS wf) $(0 + 1 + 2 + 3)\hbar\omega$ [16]	(13.2)	(12.3)
RPA	19.23	55.10
QRPA	20.29	52.0
CRPA [21]	18.18(17.80)	19.28(18.15)
EXP	$12.4 \pm 0.3 \pm 1.8$ [6], [21]	$14.1 \pm 1.6 \pm 1.9$ [8] $14.8 \pm 0.7 \pm 1.4$ [7] 14.0 ± 1.2 [9]

TABLE II. Same as table 1 for flux averaged exclusive cross sections.

	$(\nu_\mu, \mu^-)DIF$ $\langle \sigma \rangle_f (10^{-40} \text{ cm}^2)$	$(\nu_e, e^-)DAR$ $\langle \sigma \rangle_f (10^{-42} \text{ cm}^2)$
SM(HO wf) $(0 + 1 + 2)\hbar\omega$	0.70	8.42
SM(HF wf) $(0 + 1 + 2)\hbar\omega$	0.65	8.11
SM(WS wf) $(0 + 1 + 2)\hbar\omega$ [16]	0.58	8.4
RPA	2.09	49.47
QRPA	1.97	42.92
CRPA [21]	1.06(1.03)	13.88(12.55)
EXP	$0.66 \pm 1.0 \pm 1.0$ [6]	$10.5 \pm 1.0 \pm 1.0$ [8] $9.1 \pm 0.4 \pm 0.9$ [7] $9.1 \pm 0.5 \pm 0.8$ [9]

TABLE III. Same as table 1 for flux averaged inclusive cross sections but excluding the ground state.

	$(\nu_e, e^-)DAR$ $\langle \sigma \rangle_f (10^{-42} \text{ cm}^2)$
SM(HO wf) $(0 + 1 + 2)\hbar\omega$	5.79
SM(HF wf) $(0 + 1 + 2)\hbar\omega$	5.83
SM(WS wf) $(0 + 1 + 2)\hbar\omega$ [16]	3.7
SM(HF wf) $(0 + 1 + 2 + 3)\hbar\omega$	8.28
SM(HO wf) $(0 + 1 + 2 + 3)\hbar\omega$	8.31
SM(WS wf) $(0 + 1 + 2 + 3)\hbar\omega$ [16]	(3.8)
RPA	5.63
QRPA	9.08
CRPA [21]	5.4(5.6)
EXP	5.4 ± 1.9 [8]
	$5.7 \pm 0.6 \pm 0.6$ [7]
	5.1 ± 0.8 [9]

TABLE IV. ft value for the β^+ -decay from $^{12}N_{gs}$ to $^{12}C_{gs}$

	$ft(s)$
SM(HF wf) $(0 + 1 + 2)\hbar\omega$	17008
SM(HO wf) $(0 + 1 + 2)\hbar\omega$	16425
RPA	3032
EXP	$13182 \pm 1.$ [42]

TABLE V. Same as table 1 for the exclusive muon capture rates Λ_c .

	$\mu^- (^{12}C, ^{12}B_{gs})\nu_\mu$ (10^4 s^{-1})
SM(HO wf) $(0 + 1 + 2)\hbar\omega$	0.50
SM(HF wf) $(0 + 1 + 2)\hbar\omega$	0.48
SM(WS wf) $(0 + 1 + 2)\hbar\omega$ [16]	0.66
RPA	2.54
CRPA [21]	2.37(2.43)
EXP	0.62 ± 0.03 [43]

TABLE VI. Same as table 1 for the inclusive muon capture rates Λ_c .

	$\mu^- (^{12}C, ^{12}B)\nu_\mu$ (10^4 s^{-1})
SM(HF wf) $(0 + 1 + 2 + 3)\hbar\omega$	3.32
SM(WS wf) $(0 + 1 + 2 + 3)\hbar\omega$ [16]	(4.06)
RPA	5.12
CRPA [21]	5.79(5.76)
EXP	3.8 ± 0.1 [44]

TABLE VII. Contribution of the most important multipolarities J^π to the inclusive $(\nu_\mu, \mu^-)DIF$ cross sections $\langle \sigma \rangle_f$ (10^{-40} cm^2), within the RPA, QRPA and SM approaches. For the latter, results obtained with two different choices of the wavefunctions, Hartree-Fock (HF wf) and Harmonic Oscillator (HO wf) are shown.

J^π	RPA	QRPA	SM HF wf	SM HO wf
0^-	0.96	0.95	0.82	1.35
1^+	4.42	4.48	2.47	4.11
1^-	3.53	3.48	3.11	4.06
2^+	2.04	1.94	1.38	2.29
2^-	3.78	4.21	3.87	4.53
3^+	1.71	2.25	1.58	2.33
3^-	0.70	0.80	0.47	0.58
4^-	1.36	1.35	1.11	1.19

TABLE VIII. Contribution of the most important multipolarities J^π to the inclusive $(\nu_e, e^-)DAR$ cross sections $\langle \sigma \rangle_f$ (10^{-42} cm^2), within the RPA, QRPA and SM approaches. For the latter, results obtained with two different choices of the wavefunctions, Hartree-Fock (HF wf) and Harmonic Oscillator (HO wf) are shown.

J^π	RPA	QRPA	SM HF wf	SM HO wf
0^-	0.3	0.5	0.6	0.6
1^+	50.0	45.6	9.6	9.8
1^-	1.7	2.0	2.1	2.2
2^+	0.1	0.1	0.1	0.1
2^-	3.0	3.7	4.0	3.9
3^+	0.0	0.1	0.0	0.1

TABLE IX. Comparison of the the inclusive $(\nu_\mu, \mu^-)DIF$ cross sections $\langle \sigma \rangle_f$ (10^{-40} cm^2) obtained within RPA, RPA in the same model space as the SM and SM with HF wavefunctions.

J^π	RPA	RPA($3\hbar\omega$)	SM (HF wf)
0^+	0.15	0.14	0.15
0^-	0.96	0.81	0.82
1^+	4.42	3.76	2.47
1^-	3.53	3.14	3.11
2^+	2.04	1.78	1.38
2^-	3.78	3.09	3.87
3^+	1.71	1.23	1.58
3^-	0.70	0.40	0.47
4^+	0.18	0.07	0.07
4^-	1.36	1.13	1.11
5^+	0.39	0.24	0.15
6^+	0.01	0.00	0.00
TOTAL	19.23	15.79	15.18

TABLE X. Results for the different processes obtained with $g_A^{eff} = 0.9g_A$ both within RPA and SM.

		RPA	SM (HF wf)
$(\nu_\mu, \mu^-)DIF < \sigma >_f$ (10^{-40} cm^2)	exclusive	1.76	0.55
	inclusive	17.02	13.49
$(\nu_e, e^-)DAR < \sigma >_f$ (10^{-42} cm^2)	exclusive	40.79	6.69
	inclusive	45.63	13.8
ft value(s)		3743	20278
Λ_c (10^4 s^{-1})	exclusive	2.05	0.387
	inclusive	4.11	2.78

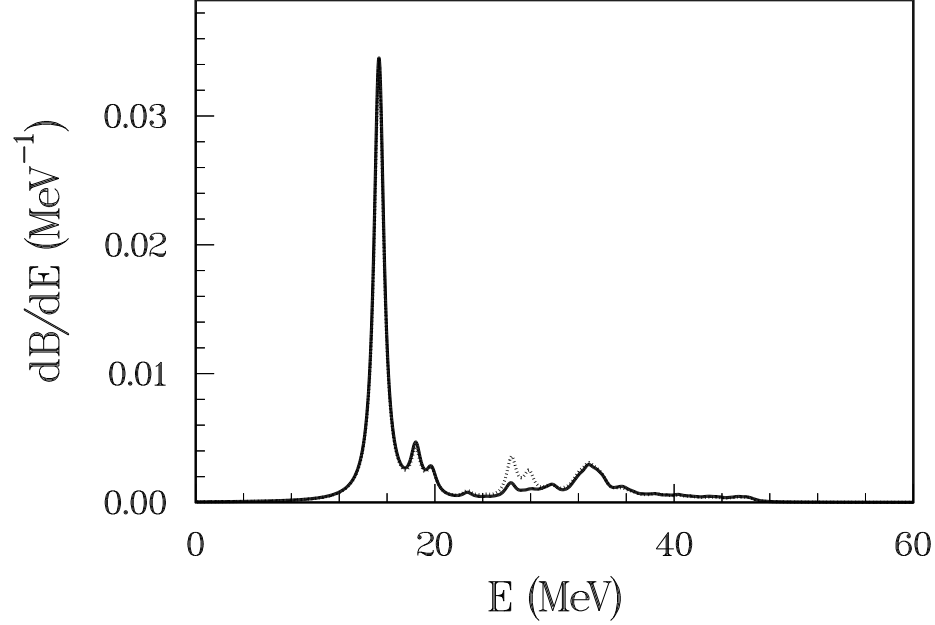


FIG. 1. Strength distributions for the $J^\pi = 1^+$ states obtained with the transition operator $\hat{O} = \sum_k t_+(k) j_0(qr_k) [Y_0(r_k) \times \sigma]^1$ with $q = 0.2 \text{ fm}^{-1}$, using both HO (full line) and HF wavefunctions (dotted line). The lines are the results of a folding with a lorentzian of 1 MeV width.

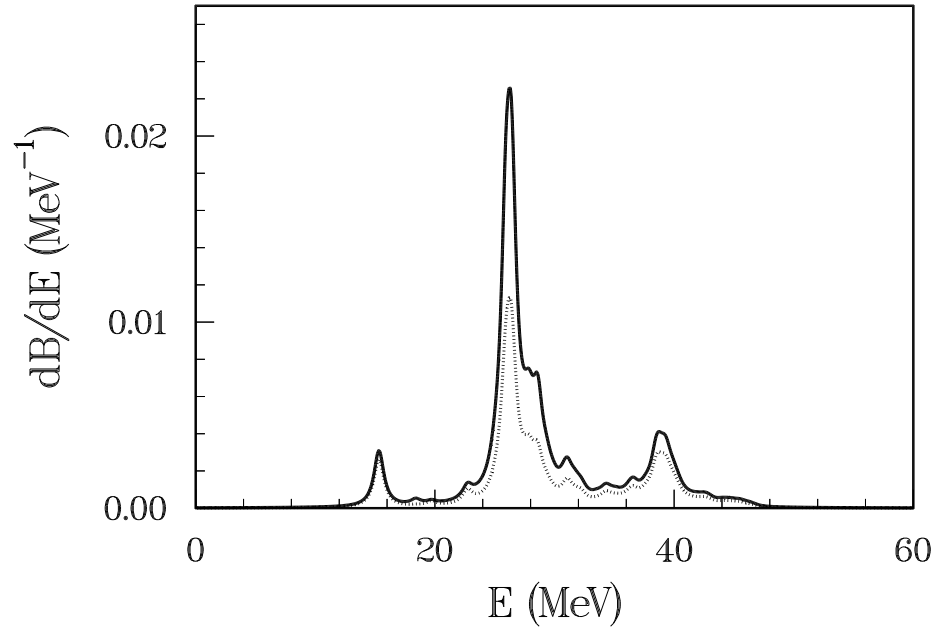


FIG. 2. Strength distributions for the $J^\pi = 1^+$ states obtained with the transition operator $\hat{O} = \sum_k t_+(k) j_0(qr_k) [Y_0(r_k) \times \sigma]^1$ with $q = 1.0 \text{ fm}^{-1}$, using both HO (full line) and HF wavefunctions (dotted line). The lines are the results of a folding with a lorentzian of 1 MeV width.

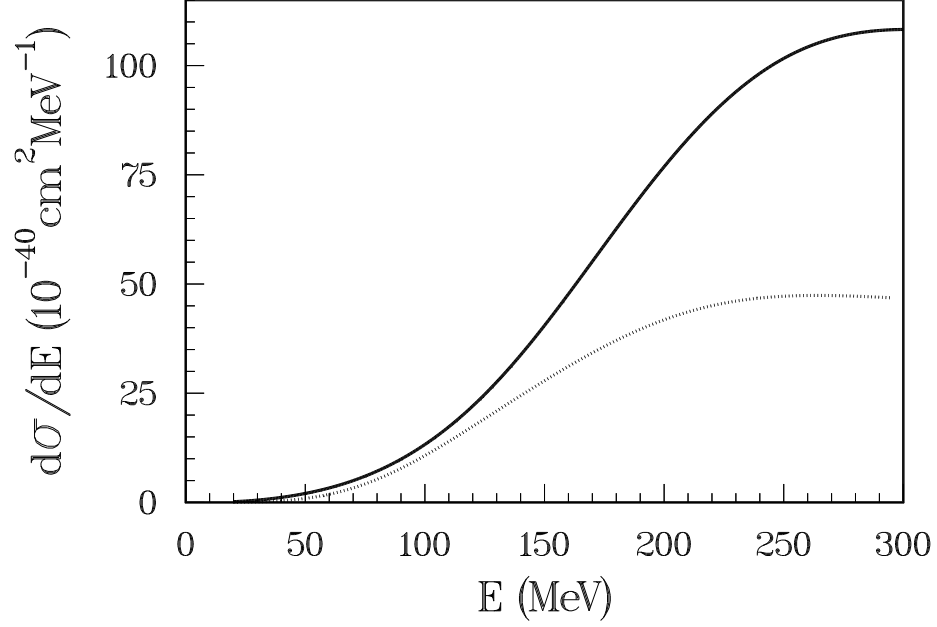


FIG. 3. Inclusive (ν_e, e^-) *DIF* differential cross section as a function of neutrino energy, calculated both in RPA (full line) and in SM (dotted line).

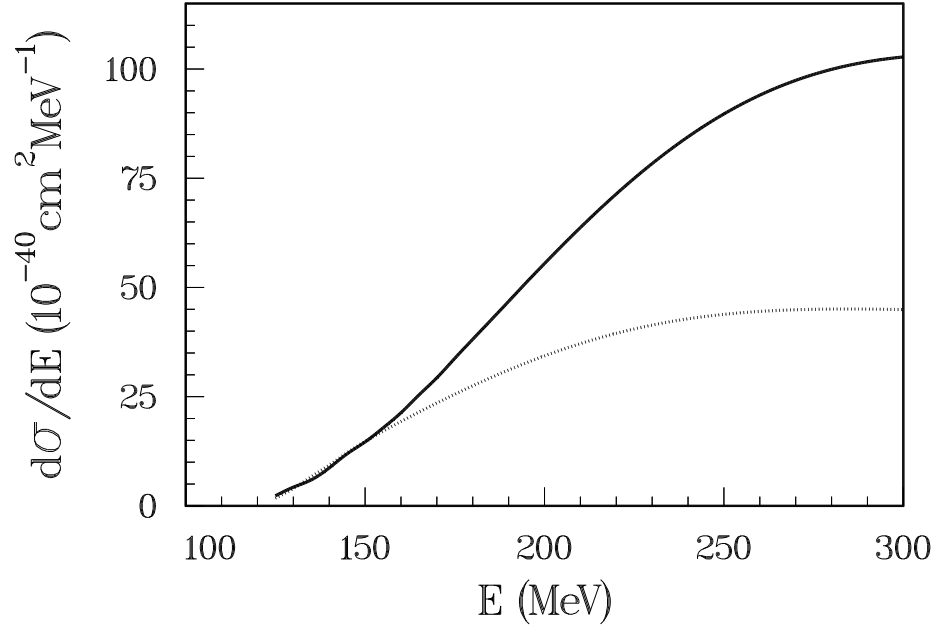


FIG. 4. Inclusive (ν_μ, μ^-) *DIF* differential cross section as a function of neutrino energy, calculated both in RPA (full line) and in SM (dotted line).

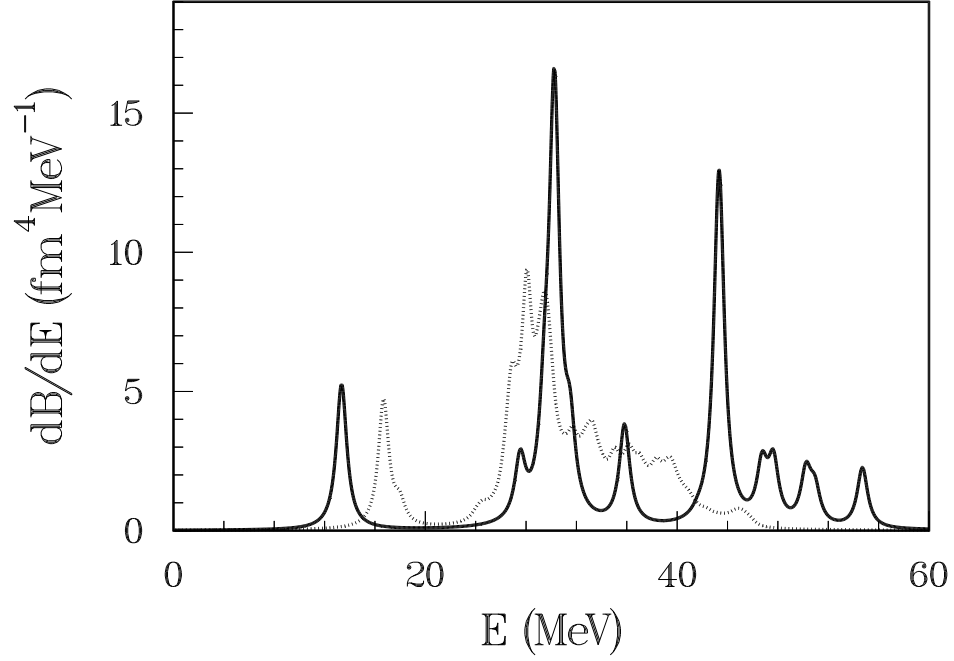


FIG. 5. Strength distributions for the $J^\pi = 2^+$ obtained with the Fermi type operator $\hat{O} = \sum_k r_k^2 Y_2(r_k) t_+(k)$ with the RPA approach (full line) and SM (dotted line). The lines are the results of a folding with a lorentzian of 1 MeV width.